Robust multimaterial tellurium-based chalcogenide glass fibers for mid-wave and long-wave infrared transmission

Guangming Tao,[1] Soroush Shabahang,[1] He Ren,[1,2] Farnood Khalilzadeh-Rezaie,[3] Robert E. Peale,[3] Zhiyong Yang,[4] Xunsi Wang,[1,5] and Ayman F. Abouraddy[1,*]

[1]*CREOL, The College of Optics & Photonics, University of Central Florida, Orlando, Florida 32816, USA*

[2]*School of Physics and Electronic Engineering, Jiangsu Normal University, Xuzhou, Jiangsu 221005, China*

[3]*Department of Physics, University of Central Florida, Orlando, Florida 32816, USA*

[4]*Laser Physics Centre, Research School of Physics and Engineering, The Australian National University, Canberra, ACT 2600, Australia*

[5]*Laboratory of Infrared Material and Devices, Advanced Technology Research Institute, Ningbo University, Ningbo, Zhejiang 315211, China*

**Corresponding author: raddy@creol.ucf.edu*

Received April 29, 2014; accepted April 30, 2014;
posted May 27, 2014 (Doc. ID 211160); published June 30, 2014

We describe an approach for producing robust multimaterial chalcogenide glass fibers for mid-wave and long-wave mid-infrared transmission. By combining the traditional rod-in-tube process with multimaterial coextrusion, we prepare a hybrid glass–polymer preform that is drawn continuously into a robust step-index fiber with a built-in, thermally compatible polymer jacket. Using tellurium-based chalcogenides, the fibers have a transparency window covering the 3–12 μm spectral range, making them particularly attractive for delivering quantum cascade laser light and in space applications. © 2014 Optical Society of America

OCIS codes: (060.0060) Fiber optics and optical communications; (120.0120) Instrumentation, measurement, and metrology; (160.0160) Materials.
http://dx.doi.org/10.1364/OL.39.004009

Progress in quantum cascade lasers (QCLs) is enabling mid-infrared (MIR) applications in sensing and spectroscopy [1], and is motivating the development of MIR optical components and devices. Applications in space science, such as the search for Earth-like planets, also require optical technologies at long-wave MIR wavelengths [2]. Fabricating *optical fibers* for this spectral range remains a multifaceted challenge involving identification of materials and fabrication strategies. Although single-crystal materials (e.g., Ge, ZnSe) and polycrystalline halides (e.g., AgBrCl, CsI) transmit light across 3–14 μm and are candidates for MIR bulk components, their crystallinity precludes thermal fiber drawing, whereas hot extrusion produces fibers of limited length, chemical stability, and mechanical strength [3]. Single-crystal sapphire fibers are produced readily [4–6] but do not transmit light beyond 4 μm, and hollow-core photonic bandgap fibers typically have narrow transmission windows [7]. Recently, fibers consisting of a semiconducting core and silica glass cladding have been demonstrated [8], but more research is needed to reduce losses and develop a MIR-transparent cladding [9].

Thermal drawing is best suited for glasses, and among MIR glasses such as tellurites, fluorides, and chalcogenides (ChGs), the latter exhibit the widest MIR transparency window [10]. In particular, tellurium-based ChG (Te-ChG) compositions may be stably drawn into fibers [11–13] and encompass the 3–5 and 8–14 μm atmospheric windows, the QCL spectral range, and CO and CO_2 lasers. Step-index Te-ChG fibers have been produced via the rod-in-tube [14] or double-crucible [15] strategy, or more specialized approaches [16] (see also the glass purification schemes for Te-ChG fibers [17–20]).

Although the rod-in-tube method typically produces higher loss due to imperfections at the core–cladding interface [14], it remains to date widely used due to its simplicity and flexibility with respect to material choices [21–23]. Nevertheless, Te-ChG fibers produced by any of these approaches remain of limited utility since they are brittle and difficult to handle without providing a plastic coating. Ideally, the coating should be thermomechanically compatible with the glass, easily applied, and induce little extra loss [24]. We recently developed a fabrication approach satisfying these desiderata via multimaterial coextrusion of a specially designed billet into a hybrid ChG–polymer preform [25]. This preform is readily drawn into a *robust* fiber provided with a thick built-in polymer jacket that does not participate in the optical functionality [26–28]. The main disadvantage of this method is the tapered internal structure of the preform, leading to a low utilization efficiency of the materials in achieving the target fiber geometry.

In this Letter, we combine multimaterial coextrusion with the rod-in-tube methodology to maximize the process yield, without compromising the fiber robustness. We implement this novel procedure using Te-ChGs from the GeAsSeTe system, which are stable against crystallization and amenable to thermal drawing, resulting in the first *robust* mid-wave and long-wave MIR fibers produced efficiently from the initial materials. These fibers may provide a simple and convenient delivery approach for QCLs and other MIR lasers.

To ensure a wide MIR transparency window, we used the ChG compositions G_1: $Ge_{20}As_{20}Te_{45}Se_{15}$ and G_2: $Ge_{20}As_{20}Te_{42}Se_{18}$ for the core and cladding, respectively. Increasing the percentage of Se and lowering that of Te in the ChG composition serves to reduce the refractive index of G_2 with respect to that of G_1. Each glass was prepared in the form of a cylindrical rod by melt-quenching [29], and the G_2 rod was annealed for

 © 2014 Optical Society of America

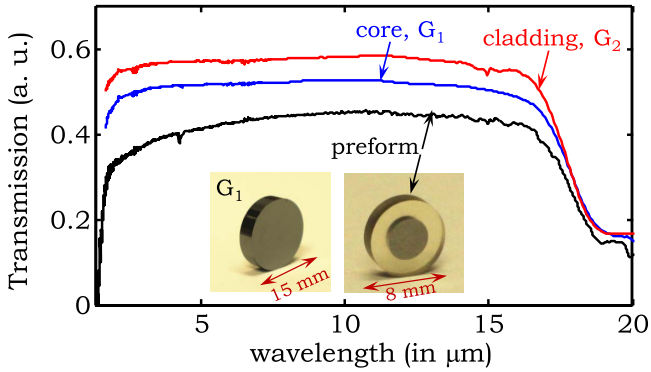

Fig. 1. FTIR transmission spectrum for bulk Te-ChG samples used as core (G_1) and cladding (G_2) in our fiber. Transmission through a 2-mm-thick disk sectioned from an extruded preform is also shown. The insets show photographs of the samples. The left inset shows a bulk disk of G_1 sectioned from a rod produced by melt-quenching [Fig. 2(b)]. The right inset shows a preform disk that was sectioned from the full extruded preform shown in Fig. 2(c).

~30–40 h to minimize internal stresses prior to mechanical drilling. The Fourier-transform IR (FTIR) transmission spectra of the two Te-ChGs in bulk form (polished 15-mm-diameter, 2-mm-thick disks) are provided in Fig. 1, confirming their broad MIR transparency. Furthermore, we measured the refractive index of the bulk glasses using spectroscopic ellipsometry. For G_1 (G_2), the index dropped from 3.252 (3.150) at 2 μm to 3.170 (3.079) and 3.158 (3.068) at 6 and 10 μm, respectively. Fresnel reflection of ~25% at a ChG–air interface, in addition to the quality of the surface polish, accounts for the transmission baseline.

To prepare the extrusion billet, a cylinder of the core glass G_1 having diameter 7.92–7.95 mm and length 19 mm was obtained by sectioning and polishing a longer cylinder. A cylindrical tube of the cladding glass G_2 having outer diameter 15 mm, inner diameter 7.95–8.00 mm, and height 22 mm was obtained by sectioning, mechanical drilling, and polishing the inner tube surface [Fig. 2(a)]. To reduce the gap between the rod and the tube resulting from machining tolerances, the rod outer surface and the tube inner surface were polished to yield slightly tapered structures. The tapered rod (G_1) is inserted into the tube (G_2) to form a rod-in-tube assembly. The tapered surfaces result in the large-diameter end of the rod protruding from the tube [Fig. 2(b)]. This assembly is placed inside the polymer sheath to form a billet for multimaterial coextrusion. The polymer sheath was produced from a polyethersulfone (PES) polymer cylinder of diameter 30 mm that was fabricated by a thin-film-rolling process [7,30], in which a 15.2-mm-diameter, 23-mm-deep stepped hole was then machined.

If we denote the core–cladding diameter ratio by y, then in Ref. [25], y extends by definition from 0 to 1 (from the beginning to the end of the extrusion, respectively). In the current approach, this issue is obviated. The small tapering angles incorporated in the inner diameter of the cladding tube and the outer diameter of the core rod [Fig. 2(b)] are negligible when compared with the results in Ref. [25]. Indeed, this tapering angle is ≈0.1° (change in diameter of 0.03 mm over a length of 19 mm). The

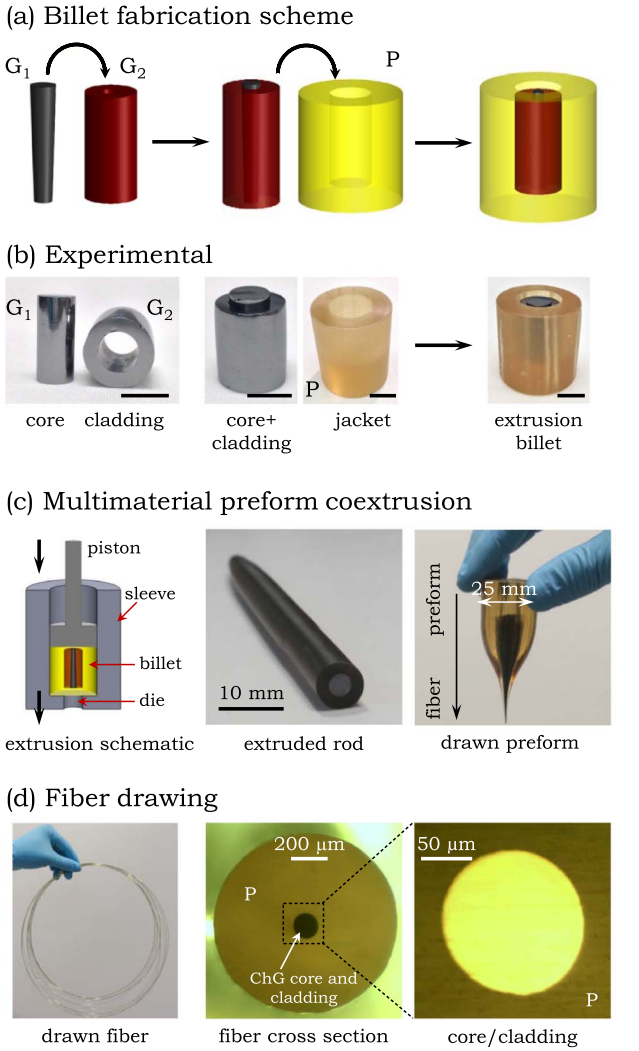

Fig. 2. Fabrication of a robust multimaterial Te-ChG fiber. (a) Schematic of the fabrication steps to produce the extrusion billet via a modified rod-in-tube process. G_1 (rod) and G_2 (tube) are the core and cladding Te-ChGs, respectively, and P is the polymer jacket. (b) Photographs of the structures corresponding to the schematics in (a), culminating in a hybrid ChG–polymer billet. All scale bars are 10 mm. (c) Extruding the billet into a rod (middle panel) and subsequent preparation of a preform (right panel). (d) Thermal drawing of the preform into an extended robust fiber. The middle panel is a transmission optical micrograph of the cross section. The right panel is a reflection optical micrograph of the Te-ChG core–cladding. The core–cladding interface is not visible due to the small index contrast.

tapered rod in the schematic in Fig. 2(a) is exaggerated for clarity. After extrusion [Fig. 2(c), middle panel], we can no longer detect that small angle.

The billet assembly is loaded into a 30-mm-diameter sleeve heated to the material softening temperature and extruded through a 6-mm-diameter circular die under 300–500 lbs of force at a speed of ~0.3–0.7 mm/min to obtain a multimaterial preform with a G_1-core, G_2-cladding, and polymer built-in jacket structure, as shown in Fig. 2(c) (middle panel). The transverse structure of the rod is uniform along its length (except for perturbations at its ends). FTIR transmission through a 2-mm-thick section of the rod is shown in Fig. 1 and is consistent with

that of the bulk ChG. The 2-mm-diameter FTIR beam was smaller than the "core" diameter in this disk, and the preform transmission spectrum in Fig. 1 thus represents only the core material G_1. The purpose of this measurement was to ensure that the thermal processing involved in extrusion does not affect the quality of the glass as reflected in the transparency window. Hence, a thin section of the preform (2 mm thick; Fig. 1, right inset) was utilized to avoid the core–cladding interface and absorption in the polymer jacket.

To prepare a preform for fiber drawing, we roll a 125-μm-thick PES film around the extruded rod and consolidate under vacuum at 245°C to form a 25-mm-diameter preform [Fig. 2(c), right panel]. This preform is drawn thermally in an ambient environment into extended lengths of robust and flexible 1-mm-outer-diameter fiber in a home-built draw tower. The glass transition temperatures of the glasses and PES are 200°C and 220°C, respectively. The fiber is drawn at a higher temperature, closer to that of the softening temperatures of the glasses and the polymer where the viscosities are closer. The length of the continuously drawn fiber is determined by the preform length and the draw-down ratio (ratio of the preform and fiber diameters). Figure 2(d) shows 7 m of the drawn fiber and its cross section. The G_1 core diameter is 70 μm and the G_2 cladding diameter is 140 μm.

We carried out optical characterization of the fiber using multiple sources throughout the spectral range of interest. We first measured the spectral transmission across MIR via FTIR. The FTIR beam was collimated using two lenses of focal lengths $f = 10$ and 6 cm, and was then focused with an aspheric $f = 6$ mm lens into the core of a 3-cm-long fiber with both facets polished [all ZnSe lenses; see Fig. 3(a), inset]. The FTIR transmission spectrum [Fig. 3(a)] reveals that the fiber has a transparency window $\lambda > 2$ μm, the transmission is flat over 3–10 μm, and that it decreases gradually at longer wavelengths as expected from the transmission spectra of the bulk glasses and the preform (Fig. 1). The transmission spectrum in the 3–12 μm spectral range is within 6 dB from the peak transmission.

Since one of the main applications of such a fiber is in QCL transmission, we measured the fiber transmission loss by the cutback technique using two QCLs with wavelengths 6.1 and 9.4 μm (ALPES Lasers, sb2481DN and sb2479UP, respectively; repetition rate of 2 kHz and pulse width of 100 ns). In addition, these measurements allow us to calibrate the FTIR-measured spectrum. A pair of aspheric ZnSe lenses was used to couple the beam to the fibers. First, a lens with $f = 6$ mm collimated the diverging QCL beam (the measured divergence angle for the QCL corresponds to a numerical aperture (NA) of 0.31); then a lens with $f = 12$ mm coupled the beam into the fiber [Fig. 3(a), inset] and the transmitted power was measured using a liquid nitrogen-cooled mercury–cadmium–telluride (MCT) detector abutted to the fiber output facet. Fresnel reflection from the air–Te-ChG interface is ~25%. An exponential fitting to the results of the cutback measurements on 1-m-long fibers yields an estimated fiber loss of ~6.1 dB/m at a wavelength of 6.1 μm and ~4 dB/m at 9.4 μm. The main origin of the losses is impurities in the starting glass material. We have

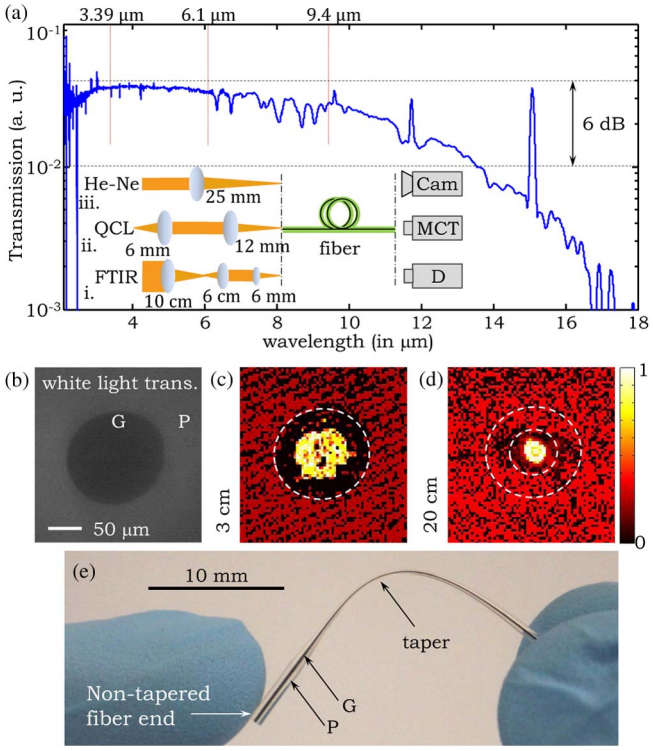

Fig. 3. (a) Transmission spectrum obtained via FTIR for a 3-cm-long fiber sample. The inset shows the three configurations used to measure the transmission of three sources; from bottom to top: (i) FTIR; (ii) QCL (at 6.1 and 9.4 μm); and (iii) a He–Ne laser (at 3.39 μm). To the left of the fiber, we show the coupling system for each source and to the right, we show the corresponding detector. The numbers refer to the focal length of each lens. Here "D" is a DLaTGS detector and "Cam" is an IR camera. (b) White light transmission image through a fiber sample. (c) and (d) IR field distribution through 3- and 20-cm-long fibers. The white-dashed circles are guides for the eye and correspond to the core–cladding and cladding–jacket interfaces. (e) Photograph of a multimaterial Te-ChG fiber tapered by a factor of 3, demonstrating its mechanical robustness. The black Te-ChG core and cladding are visible inside the transparent polymer jacket.

not implemented the purification and distillation steps that are typically used to reduce impurities in ChGs [31]. The measured divergence of the mode emerging from a 20-cm-long fiber corresponds to a NA of 0.26 (corresponding to a V number of 9.7). This NA value is smaller than expected from the index measurements of G_1 and G_2, indicating the need for more precise IR index measurements.

Finally, we determined the mode profile in the fiber using a 3.39-μm-wavelength collimated He–Ne laser (Research Electro-Optics, model 32172) focused into the fiber using a $f = 25$ mm lens and the output field was imaged via a $f = 6$ mm lens to an IR camera (Pyrocam III). A white light transmission image [captured using a MicronViewer 7290A camera; Fig. 3(b)] identifies the interface between the glass cladding and the polymer jacket. The small index contrast between the core and cladding glasses (G_1 and G_2) and their opacity in the visible prevent identifying the core–cladding interface, whereas the IR image at 3.39 μm helps identifying the core. In Figs. 3(c) and 3(d), we show the measured

distribution from 3- and 20-cm-long fiber sections. It is clear that the fiber at this wavelength is not in the single-mode regime, but modal filtering over a sufficient fiber length isolates the fundamental mode.

A major advantage of this fiber over Te-ChG fibers prepared using alternative methodologies is in its superior mechanical characteristics stemming from the built-in polymer jacket, which we have characterized elsewhere [25,26]. Furthermore, the fiber may be tapered without removing the jacket since the Te-ChG and the polymer are thermally compatible, thereby yielding robust tapers for potential long-wave MIR nonlinear fiber optics that would benefit from the high optical nonlinearities of these ChGs [32]. A taper is shown in Fig. 3(e), highlighting its mechanical robustness. The 1-mm-diameter fiber is tapered to reach a diameter of 320 μm (the corresponding core diameter is ~22 μm). For an 18-cm-long taper sample, transmission loss increased by less than 50% with respect to that of the un-tapered fiber (measurement carried out at a wavelength of 6.1 μm).

In conclusion, we have demonstrated a fabrication approach for robust mid-wave and long-wave MIR fibers using Te-ChG glasses. The multimaterial fiber is drawn continuously from a hybrid glass–polymer preform obtained by extruding a composite rod-in-tube billet assembly. The resulting fiber is robust yet flexible, and maintains low loss across the 3–12 μm spectral window, making it an attractive prospect for transmitting QCL light, for fiber telescopes used in the search for extrasolar planets [33], and, potentially, to pave the way for long-wave MIR nonlinear fiber applications.

This work was supported by the U.S. National Science Foundation (ECCS-1002295). Dr. Z. Yang is supported by ARC DECRA project DE120101036.

References

1. F. Capasso, Opt. Eng. **49**, 111102 (2010).
2. L. Kaltenegger and M. Fridlund, Adv. Space Res. **36**, 1114 (2005).
3. J. A. Harrington, Appl. Opt. **27**, 3097 (1988).
4. R. K. Nubling and J. A. Harrington, Appl. Opt. **36**, 5934 (1997).
5. D. C. Harris, Proc. SPIE **7425**, 74250P (2009).
6. M. R. B. Andreeta and A. C. Hernandes, in *Springer Handbook of Crystal Growth*, G. Dhanaraj, K. Byrappa, V. Prasad, and M. Dudley, eds. (Springer, 2010), pp. 393–432.
7. A. F. Abouraddy, M. Bayindir, G. Benoit, S. D. Hart, K. Kuriki, N. Orf, O. Shapira, F. Sorin, B. Temelkuran, and Y. Fink, Nat. Mater. **6**, 336 (2007).
8. J. Ballato, T. Hawkins, P. Foy, B. Yazgan-Kokuoz, R. Stolen, C. McMillen, N. K. Hon, B. Jalali, and R. Rice, Opt. Express **17**, 8029 (2009).
9. J. Ballato and P. Dragic, J. Am. Ceram. Soc. **96**, 2675 (2013).
10. B. J. Eggleton, B. Luther-Davies, and K. Richardson, Nat. Photonics **5**, 141 (2011).
11. T. Katsuyama and H. Matsumura, Appl. Phys. Lett. **49**, 22 (1986).
12. J. Nishii, S. Morimoto, I. Inagawa, R. Iizuka, T. Yamashita, and T. Yamagishi, J. Non-Cryst. Solids **140**, 199 (1992).
13. J. S. Sanghera, V. Q. Nguyen, P. C. Pureza, F. H. Kung, R. Miklos, and I. D. Aggarwal, J. Lightwave Technol. **12**, 737 (1994).
14. J. Nishii, T. Yamashita, and T. Yamagishi, Appl. Opt. **28**, 5122 (1989).
15. M. F. Churbanov, V. S. Shiryaev, A. I. Suchkov, A. A. Pushkin, V. V. Gerasimenko, R. M. Shaposhnikov, E. M. Dianov, V. G. Plotnichenko, V. V. Koltashev, Y. N. Pyrkov, J. Lucas, and J.-L. Adam, Inorg. Mater. **43**, 441 (2007).
16. D. L. Coq, C. Boussard-Plédel, G. Fonteneau, T. Pain, B. Bureau, and J.-L. Adam, J. Non-Cryst. Solids **326**, 451 (2003).
17. S. Danto, P. Houizot, C. Boussard-Pledel, X. H. Zhang, F. Smektala, and J. Lucas, Adv. Funct. Mater. **16**, 1847 (2006).
18. A. A. Wilhelm, C. Boussard-Plédel, Q. Coulombier, J. Lucas, B. Bureau, and P. Lucas, Adv. Mater. **19**, 3796 (2007).
19. X. Wang, Q. Nie, G. Wang, J. Sun, B. Song, S. Dai, X. Zhang, B. Bureau, C. Boussard, C. Conseil, and H. Ma, Spectrochim. Acta, Part A **86**, 586 (2012).
20. C. Conseil, J.-C. Bastien, C. Boussard-Plédel, X.-H. Zhang, P. Lucas, S. Dai, J. Lucas, and B. Bureau, Opt. Mater. Express **2**, 1470 (2012).
21. P. Houizot, C. Boussard-Plédel, A. J. Faber, L. K. Cheng, B. Bureau, P. A. V. Nijnatten, W. L. M. Gielesen, J. P. do Carmo, and J. Lucas, Opt. Express **15**, 12529 (2007).
22. Z. Yang, T. Luo, S. Jiang, J. Geng, and P. Lucas, Opt. Lett. **35**, 3360 (2010).
23. S. Maurugeon, C. Boussard-Plédel, J. Troles, A. J. Faber, P. Lucas, X. H. Zhang, J. Lucas, and B. Bureau, J. Lightwave Technol. **28**, 3358 (2010).
24. M. Wehr and C. L. Sergent, Proc. SPIE **0618**, 130 (1986).
25. G. Tao, S. Shabahang, E.-H. Banaei, J. J. Kaufman, and A. F. Abouraddy, Opt. Lett. **37**, 2751 (2012).
26. S. Shabahang, M. P. Marquez, G. Tao, M. U. Piracha, D. Nguyen, P. J. Delfyett, and A. F. Abouraddy, Opt. Lett. **37**, 4639 (2012).
27. S. Shabahang, G. Tao, J. J. Kaufman, and A. F. Abouraddy, J. Opt. Soc. Am. B **30**, 2498 (2013).
28. S. Shabahang, G. Tao, M. P. Marquez, H. Hu, T. R. Ensley, P. J. Delfyett, and A. F. Abouraddy, J. Opt. Soc. Am. B **31**, 450 (2014).
29. G. Tao, H. Guo, L. Feng, M. Lu, W. Wei, and B. Peng, J. Am. Ceram. Soc. **92**, 2226 (2009).
30. G. Tao, A. M. Stolyarov, and A. F. Abouraddy, Int. J. Appl. Glass Sci. **3**, 349 (2012).
31. G. E. Snopatin, V. S. Shiryaev, V. G. Plotnichenko, E. M. Dianov, and M. F. Churbanov, Inorg. Mater. **45**, 1439 (2009).
32. S. Cherukulappurath, M. Guignard, C. Marchand, F. Smektala, and G. Boudebs, Opt. Commun. **242**, 313 (2004).
33. F. Hénault, Opt. Lett. **34**, 1096 (2009).